Near-threshold fatigue crack growth in bulk metallic glass composites

Kombaiah Boopathy
Department of Materials Engineering, Indian Institute of Science, Bangalore-560012, India

Douglas C. Hofmann
Keck Laboratory for Engineering Materials, California Institute of Technology, Pasadena, California 91125; and Liquidmetal Technologies, 30452 Esperanza, Rancho Santa Margarita California 92688

William L. Johnson
Keck Laboratory for Engineering Materials, California Institute of Technology, Pasadena, California 91125

Upadrasta Ramamurty[a)]
Department of Materials Engineering, Indian Institute of Science, Bangalore-560012, India

(Received 14 August 2009; accepted 22 September 2009)

A major drawback in using bulk metallic glasses (BMGs) as structural materials is their extremely poor fatigue performance. One way to alleviate this problem is through the composite route, in which second phases are introduced into the glass to arrest crack growth. In this paper, the fatigue crack growth behavior of in situ reinforced BMGs with crystalline dendrites, which are tailored to impart significant ductility and toughness to the BMG, was investigated. Three composites, all with equal volume fraction of dendrite phases, were examined to assess the influence of chemical composition on the near-threshold fatigue crack growth characteristics. While the ductility is enhanced at the cost of yield strength vis-à-vis that of the fully amorphous BMG, the threshold stress intensity factor range for fatigue crack initiation in composites was found to be enhanced by more than 100%. Crack blunting and trapping by the dendritic phases and constraining of the shear bands within the interdendritic regions are the micromechanisms responsible for this enhanced fatigue crack growth resistance.

I. INTRODUCTION

Bulk metallic gasses (BMGs) have many attractive mechanical properties that include high values of stiffness, strength, hardness, and crack initiation toughness. However, lack of ductility and crack growth resistance and extremely poor fatigue properties are some of the major impediments for widespread structural applications of these materials.[1] Plastic deformation in BMGs at low temperatures (i.e., at temperature below 70% of the glass transition temperature, T_g) occurs through localization of shear into narrow bands, referred to as shear bands.[1] In the absence of a microstructure, shear bands propagate unhindered, ultimately leading to failure. This is the reason for poor ductility in monotonic loading of unconstrained BMG specimens. Under cyclic loading, shear bands form at relatively low stresses (sometimes as low as 10% of the tensile strength of the BMG) and become crack initiation sites that grow under fatigue loading, leading to relatively low endurance limits vis-à-vis crystalline metals and alloys.[2] Consequently, improving fatigue performance of BMGs has been a major area of recent research.

One way of enhancing the fatigue resistance of BMGs is to introduce compressive residual the stresses at the surfaces, which can be accomplished through a shot-peening process.[3] However, unlike crystalline alloys, (steels are a classic example) where there is a synergistic interaction between residual stresses and work hardening of the surface layers, strain softening in BMGs counteracts the potential benefit of compressive residual stresses.[4,5] Therefore, no net enhancement in fatigue life could be obtained through this method.[3]

The second and more obvious option to improve fatigue life is to introduce a "microstructure" to the BMG. This can be done in a number of different ways. One is to crystallize the BMG by annealing it above its T_g. However, this process severely embrittles the alloy and hence is not viable.[6–9] Ex situ reinforcements have also been tried, but problems with porosity and glass/particle interfaces typically prevent significant improvement over the monolithic glass.[10] Yet another approach is to allow for crystalline dendrite formation in situ during cooling.[11–14] In this strategy, controlling the interdendrite spacing throughout the sample is critical for toughening, as the cooling rates at the surface and interior of the sample could differ significantly.[15] This problem was solved by Hofmann et al.[15] who designed the processing in such a

[a)]Address all correspondence to this author.
e-mail: ramu@materials.iisc.ernet.in
DOI: 10.1557/JMR.2009.0439

 © 2009 Materials Research Society

way that the dendrites precipitate when the BMG is in the semi-solid state and then the alloy is cooled to vitrify the remaining liquid. The processing parameters are controlled such that the resulting microstructure is optimized in terms of second-phase volume fraction, morphology, and length. In particular, this approach ensures that the interdendrite spacing is less than the critical length scale required for shear-band initiated fracture, thus allowing for processing of BMG composites with a tensile ductility of >10% and mode I notch fracture toughness up to ~170 MPa·m$^{1/2}$.[15] Recently, Launey et al.[16] showed through the fracture resistance curves measured in terms of the *J*-integral that these BMG matrix composites exhibit fracture toughness up to 150 to 200 MPa·m$^{1/2}$, which is 3 to 4 times higher than that of as-cast BMG with similar composition.

In general, the nonlinear deformation that enhances quasi-static toughness of a material also leads to lowered fatigue resistance.[17] Therefore, how these newly developed BMG composites fare, in terms of fatigue, is an issue of importance, especially given the extremely poor fatigue characteristics of monolithic BMGs. Flores et al.,[18] who have examined the fatigue crack growth behavior of a BMG composite with 25 vol% of secondary ductile phase (referred to as LM2), reported that the threshold stress intensity range for fatigue crack initiation, ΔK_0, is similar to that of the monolithic BMG. In contrast, Wang et al.[19] report that the secondary phase deteriorates the fatigue endurance limit of BMGs. It should be noted that the composites examined by these two groups tend to have microstructures with highly variable length scales, which may be a possible reason for the discrepancy.

Recently, Launey et al.[20] examined the unnotched fatigue response (stress–life or S–N approach) of a semi-solidly processed BMG matrix composite with nominal composition of $Zr_{40}Ti_{34}Nb_{7.6}Cu_{6.4}Be_{12.5}$, developed by Hofmann et al.,[15] and show that it has remarkably higher fatigue limit than monolithic BMGs, and even better than some steel and aluminum alloys. However, reliable structural design strategies require characterization of a material through the fracture mechanics approach (also referred to as defect tolerant approach), as the S–N approach is highly sensitive to experimental parameters such as the type of loading applied, surface conditions of the specimens, and the casting defects in them. With this in mind, we evaluate the fatigue crack growth behavior of these newly developed BMG composites in an attempt to examine how the ductile phase affects fatigue crack growth, particularly near the threshold. An additional, and important, objective of this work is to examine the compositional effect on fatigue behavior of Zr–Ti–Nb–Cu–Be BMG composites. To this end, the composition of the glass matrix and the dendrite were systematically altered by varying the Zr/Ti ratio while holding Nb, Cu, and Be compositions constant, as all three elements chemically partition in the alloy. This was accomplished without changing the overall volume fraction of second phase. This allowed us to investigate the fatigue crack growth behavior of three similar composites, one Zr-rich, one Ti-rich, and one with Zr and Ti approximately equal composition, and examine the role of matrix and dendrite properties on fatigue performance.

II. MATERIALS AND EXPERIMENTS

Three different BMG composites were examined in this work; the chemical compositions are given in Table I. These composites are referred to as DH1, DH1A, and DH1B hereafter. While DH1 has near-equal Ti and Zr contents, DH1A is Ti-rich whereas DH1B is Zr-rich. They were processed semisolidly to achieve a uniform dendrite length and interdendrite spacing.[15] The solid alloy was heated to the semisolid region between the solidus and liquidus temperatures and held isothermally for several minutes to attain homogeneity. Then the semisolid liquid was quenched rapidly to vitrify the remaining liquid into a glass (~100 K/s). Further processing details can be found in references.[15,22] The processing was carried out in such a way that all the three composites contain ~0.60 volume fraction of glass, allowing for direct comparison of the compositional effect without the varying volume fractions complicating it.

Samples were cut from the ingots through electro-discharge machining and were mirror polished and etched by Kroll's reagent (10 mL HNO_3 + 5 mL HF + 85 mL H_2O) for optical microscopy. X-ray diffraction was conducted on the BMG matrix composites to detect the presence of crystalline phases by Panalytical x-ray diffractometer using Cu Kα radiation. Chemical

TABLE I. Compositions, amorphous matrix volume fractions, and quasi-static mechanical properties of the three composites examined.

Material	Composition (at.%)	V_f (%)	σ_y (MPa)	σ_f (MPa)	ε_f (%)
DH1	$Ti_{31.4}Zr_{36.6}Nb_7Cu_{5.9}Be_{19.1}$	58.0	1204 ± 88	1701 ± 98	19.6
DH1A	$Ti_{43}Zr_{25}Nb_7Cu_6Be_{19}$	61.6	1163 ± 38	1602 ± 42	13.9
DH1B	$Ti_{25}Zr_{43}Nb_7Cu_6Be_{19}$	57.0	1071 ± 11	1503 ± 41	19.6
Vitreloy 1[2,21]	$Zr_{41.2}Ti_{13.8}Cu_{12.5}Ni_{10}Be_{22.5}$	100	1900	1900	2

V_f, volume fraction of the amorphous matrix; σ_y, yield strength; σ_f, fracture strength; ε_f, failure strain.

composition of the dendritic phase was evaluated by energy dispersive x-ray spectroscopy (EDX).

Uniaxial compression tests were performed, primarily to estimate the yield strength, σ_y, of the composites on cylindrical samples of 2.5 mm diameter and 4.5 mm length that were cut from cast ingots using EDM wire cutting. Compression tests were carried out in a Zwick screw-driven machine at a strain rate of 10^{-3} s^{-1}. All the tests were conducted up to the sample fracture. In each case, three tests were performed. Since it was not possible to mount an extensometer on these relatively short specimens, the cross-head displacement, after correcting for the machine compliance, was converted into strains. Hence, these are only nominal strains.

Fatigue crack growth studies were conducted on notched four-point bend flexure specimens with dimensions of 40 (length) × 6 (width) × 3 (thickness) mm^3. An edge notch that has a width of 80 μm and depth 2.1 mm was cut in these by EDM wire cutting, giving a starting *a*/*W* ratio of 0.35. The outer and inner span lengths of the four-point loading were 30 and 15 mm, respectively. Both sides of the fatigue samples were polished to 1 μm finish using diamond suspension and one side of the specimen was etched with Kroll's reagent so as to observe the crack's interaction with the microstructure. The specimens were precracked first by fatigue loading (maximum of the cyclic load between 400 and 700 N). These loads correspond, approximately, to ΔK ~10 to 15 MPa·$m^{1/2}$ for the initial notch length. After a crack initiates at the notch root and grows to ~200 μm, the threshold stress intensity factor range, ΔK_0, was determined by employing the load shedding method,[23] wherein the applied stress intensity range ΔK was reduced by 1 MPa·$m^{1/2}$ for a particular number of applied load cycles. The ΔK_0 value was obtained when the crack growth rate is approximately 10^{-10} m/cycle or less.

After obtaining the ΔK_0, ΔK was periodically increased and crack growth was measured. For all the fatigue crack growth experiments, the load ratio, *R* (defined as the ratio of minimum to the maximum load of the fatigue cycle) and frequency were maintained at 0.1 and 10 Hz, respectively. All the tests were performed in air and at room temperature (~23 °C). The crack growth was monitored by a high-magnification optical microscope that is capable of measuring crack extension in excess of 2 μm. The crack growth rates, *da*/*dN*, was estimated by dividing the crack length increment during a predetermined interval with the number of cycles, *N*, applied during that interval. To analyze how the crack propagates along amorphous matrix and dendrites, tests were intermittently stopped and images were taken using scanning electron microscopy (SEM). Fractography on the broken specimens was also performed on fractured samples using SEM.

III. RESULTS

A. Microstructures

Representative optical micrographs of the BMG composites are given in Fig. 1, which show body-centered cubic (bcc) dendrites in a continuous amorphous matrix. The dendrite arm spacing in all the composites is ~1 to 2 μm, and the interdendrite distance varies between 10 and 15 μm. The dendrite volume fraction, estimated using

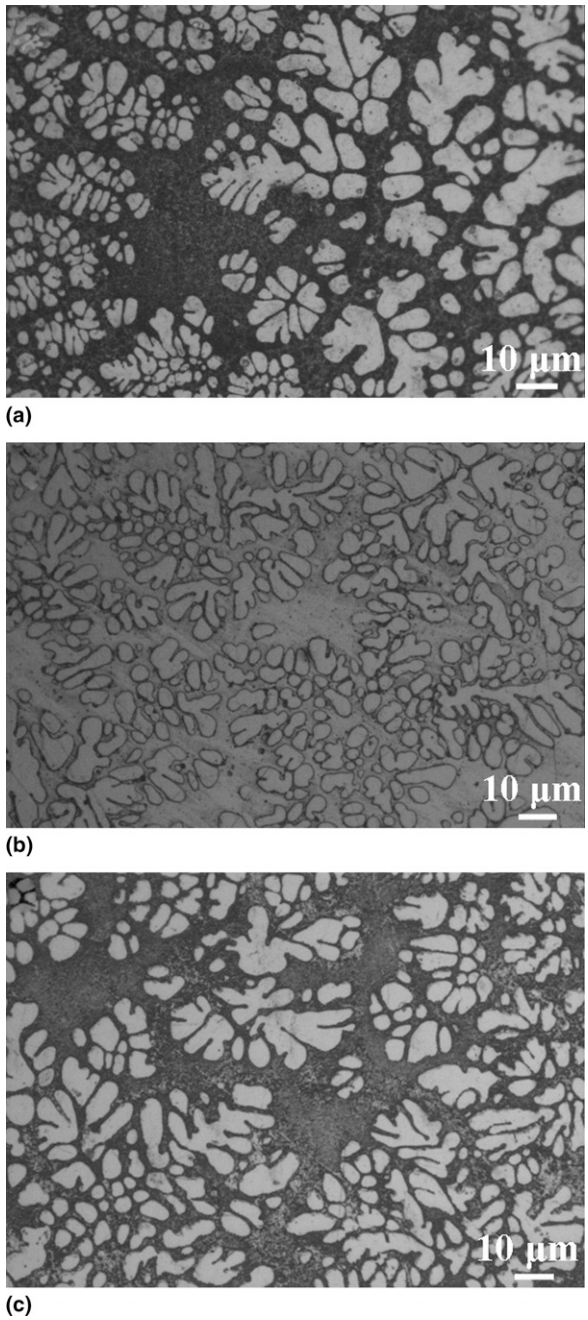

FIG. 1. Optical micrographs of BMG composites (a) DH1, (b) DH1A, and (c) DH1B, showing dendrites distributed in the amorphous matrix. The contrast difference in (b) is caused by the Ti-based dendrites, which have different *Z* contrast than the Zr-based ones.

Sigmascan image analysis, is ~40% in all the composites in our present study. The chemical compositions of the dendrites, determined using electron-dispersive x-ray analysis (EDX), are $Ti_{45}Zr_{40}Nb_{14}Cu_1$ for DH1, $Ti_{65}Zr_{20}Nb_{14}Cu_1$ for DH1A, and $Ti_{20}Zr_{65}Nb_{14}Cu_1$ for DH1B. These compositional changes are reflected in the change of contrast between these three alloys.

X-ray diffraction (XRD) patterns of the BMG composites contain peaks that clearly indicate the presence of the crystalline phase. Figure 2 shows the x-ray diffraction pattern of the BMG matrix composites in comparison with a monolithic BMG, Vit-1. (In all cases, Vit-1 was used as a baseline). The peaks in the XRD pattern are identified to be bcc β Ti–Zr–Nb phase. There is a slight shift in diffraction angle for all the three BMG matrix composites, which is a result of a change in the lattice parameter caused by compositional variation. The XRD pattern of a fully amorphous BMG shows only two broad peaks that are characteristic of amorphous materials.

B. Mechanical properties

The engineering stress–strain curves obtained under uniaxial compression are shown in Fig. 3. In general, all the three composites exhibit a distinct yield followed by considerable plasticity, with the samples failing between nominal strains of 14% and 19%. This enhancement in plastic deformation (compared with that of fully amorphous alloys that show limited plasticity even in compression[24]) comes at the expense of the σ_y. For example, the fully amorphous Zr-based BMG, Vitreloy-1 has a σ_y of ~1.9 GPa, whereas the composites tested here have σ_y ranging from 1 to 1.2 GPa. However, fully amorphous alloys are elastic-perfectly plastic; that is, they show no work hardening.[24] As a result, their fracture strength is the same as σ_y. In contrast, the composites exhibit nominal work-hardening behavior in compression, so the stress at failure ranges between 1.5 and 1.7 GPa. (Since the experiments are conducted in compression, these are not the ultimate tensile strengths and are only indicative stress values at failure.) Although fully amorphous alloys do not exhibit any work hardening, the observed strain hardening in the case of the composites is caused by the increased plastic flow resistance of the crystalline dendrites that yield first, but work harden substantially. The failure stress of 1.7 GPa, which is for DH1 alloy, is only ~10% lower than that of Vitreloy-1. These results are summarized in Table I. It is observed that among the composites, the strength increases as Ti/Zr is increased from ~0.6 to ~1.0, but does not change afterward.

Fatigue crack growth data obtained on the BMG matrix composites are shown in Fig. 4, represented as crack growth rate per cycle, *da*/*dN*, versus the stress intensity factor range, Δ*K*, plots. All three composites exhibit broadly similar fatigue crack growth response, with stable crack growth occurring over a significant range of Δ*K* values, similar to what is observed in ductile metals and alloys.

Fatigue crack growth behavior can be classified into three distinct regimes, near-threshold, steady-state (or Paris), and fast fracture regimes. Because of the small sample size and extensive crack blunting at higher Δ*K* values (>16–19 MPa·m$^{1/2}$), we could not obtain meaningful data for the fast fracture regime, which would indicate the fracture toughness of the material. However, for the near-threshold and early part of the Paris regimes, the plane strain conditions are satisfied and hence these data are used for further analysis.

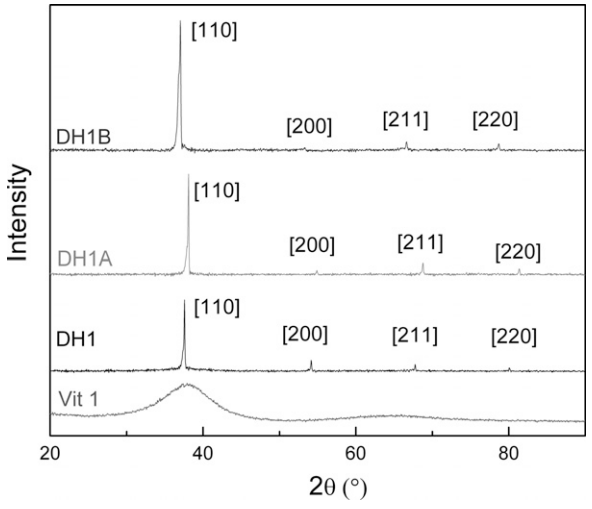

FIG. 2. X-ray diffraction (XRD) patterns of BMG matrix composites. For comparison purposes, an XRD pattern obtained on fully amorphous BMG, Vitrelloy-1 is also shown.

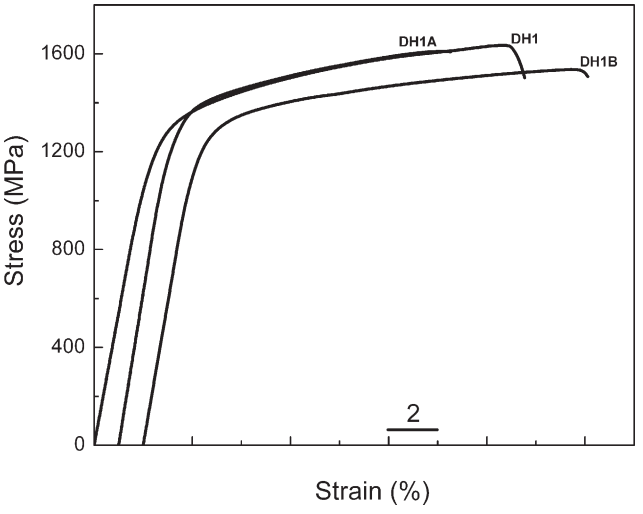

FIG. 3. Compressive stress-strain responses of the three BMG matrix composites tested at room temperature at a strain rate of 10^{-3} s^{-1}.

The fatigue crack growth response in the intermediate regime of steady-state crack growth can be characterized using the Paris law,

$$\frac{da}{dN} = C(\Delta K)^m \quad , \tag{1}$$

where C and m are material constants, with the exponent m often referred to as the Paris exponent. For ductile metals, m ranges between 2 and 4. Values of C, m, and ΔK_0 obtained on the three composites are listed in Table II. Variation of m and ΔK_0 with the composition, in terms of Ti/Zr ratio, are plotted in Fig. 5. Here, data for the monolithic BMG, Vitreloy 1, which is a widely studied BMG, were also plotted for comparison. It is clear from these plots that the fatigue crack growth resistance of BMG composites examined in this work is far superior compared with that of the fully amorphous BMG (Vitreloy 1) or its composite with 25 vol% of second phase,[2,18,25] with ΔK_0 of the composites examined in this study being larger by at least 100%. The m values recorded in the composites are much larger, closer to 4 in the case of the Zr-rich alloy whereas it is closer to 2 in the case of Vit-1. This suggests that while fatigue crack initiation is much more difficult in the composites, its steady-state growth is comparatively faster. Additionally, m and ΔK_0 values for 300-M high-strength steel and age-hardened aluminum alloy (2090-T81), taken from literature, are given in Table II. Interestingly, our BMG composites have higher ΔK_0 than all these alloys.

Within the composites examined, the ΔK_0 value for the Zr-rich composite is slightly higher than the other two compositions, which have similar ΔK_0 values. A gradual reduction in m with increasing Ti content, from a value close to 4 to 2.5, was observed.

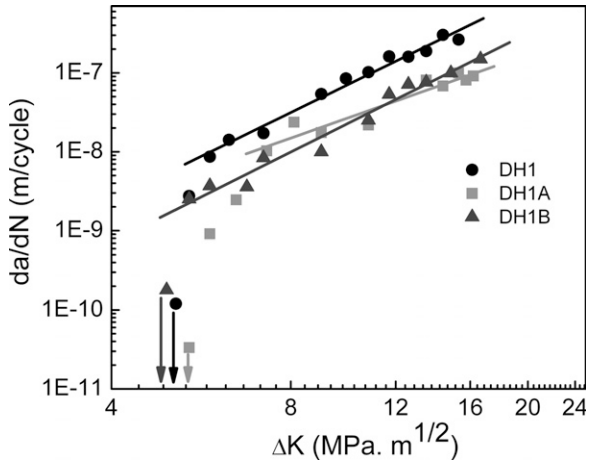

FIG. 4. Variation of the crack growth rate under cycling loading, da/dN, as a function of the applied stress intensity factor range, ΔK, for the three BMG composites examined in this study. Arrows indicate to the threshold values.

C. Micromechanisms of crack growth

Figures 6 and 7 show several micrographs obtained from the fatigued samples that were unloaded once the threshold limit was reached and examined using SEM. Figure 6 shows an image of the shear bands getting confined by the dendrites. Figure 7 shows the crack interaction with the dendritic phase, illustrating the fact that ductile dendrite phase effectively blunts the crack tip and through this process hinders its propagation. Additionally, the high-magnification SEM image of DH1 [Fig. 7(b)] shows traces of plastic deformation at the crack tip, which shows effective arrest of slip on a shear band. Plastic deformation of dendrites could also lead to work hardening, further stabilizing crack growth. The SEM images suggest that there is crack branching caused by presence of second phases near the threshold. This could result in roughness-induced crack closure. Figure 7 also shows that the fatigue crack behavior is similar in all three of the composites, indicating that they fatigue with similar characteristics, even though they vary in composition from Ti-based [Fig. 7(c)] to Zr-based [Fig. 7(d)].

In the Paris regime, the plastic deformation in BMGs is manifested by the formation of shear bands oriented nearly parallel to the crack growth direction, as shown in

TABLE II. Fatigue crack growth parameters and densities of the BMG matrix composites tested in this work. Data for Vitreloy 1 and several crystalline alloys, taken from literature, are also given for comparison.

Material	ΔK_0 (MPa·m$^{1/2}$)	m	C (MPa·m$^{1/2}$)	Density (g/cm^3)
DH1 composite	5.0	3.5	1.5×10^{-11}	5.58
DH1A composite	5.4	2.4	5.9×10^{-11}	5.43
DH1B composite	5.7	3.5	3.2×10^{-12}	5.85
Vitreloy 1[2]	1–3	2.7–4.9	1.7×10^{-13} to 1.6×10^{-11}	6.05
Vitreloy 1[25]	1.5	1.5	···	6.05
Vitreloy 1 composite (LM2)[18]	1.2	1.8	···	···
300-M Steel[2]	3	2–4	···	7.9
2090-T81 Al alloys[2]	2.1	2–4	···	2.7

ΔK_0, threshold stress intensity factor range for fatigue crack initiation; m, Paris exponent.

Fig. 8(a). The crack propagation in the amorphous matrix occurs through these shear bands. Crack growth along the matrix/dendrite interface [Fig. 8(b)] or through interpenetration of dendrites also occurs [Fig. 8(c)]. A number of factors such as the angle of crack incidence, the elastic mismatch across the interface, and the ratio of interfacial toughness determine the path of the crack.[20]

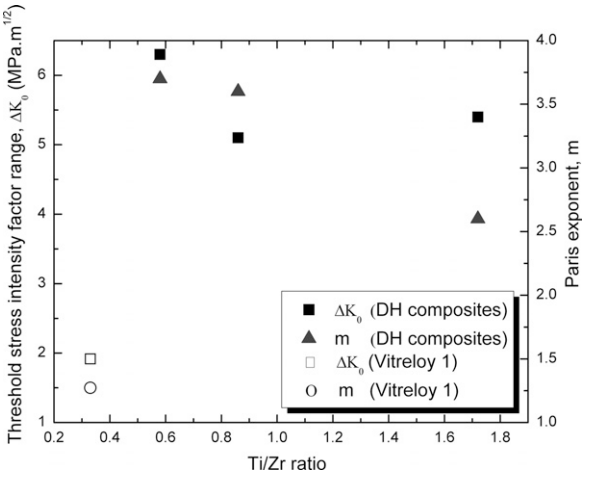

FIG. 5. Variation of the threshold stress intensity factor range for fatigue crack growth, ΔK_0, and the Paris exponent, m, plotted as a function of the Ti/Zr ratio. Data obtained by Zhang et al.[23] on fully amorphous Zr-based BMG, Vitrelloy 1, are also plotted for comparison purposes.

It is inferred from scanning electron micrographs that at higher incidence angles the crack penetrates through the dendrites, while at lower incidence angles the crack gets deflected and passes through interface of dendrites and matrix.

Fractographs obtained from the samples that fractured into two pieces are shown in Fig. 9. These images clearly show the presence of fatigue striations on both the amorphous matrix and dendrite in all the composites. However, the striation spacing is much coarser in the

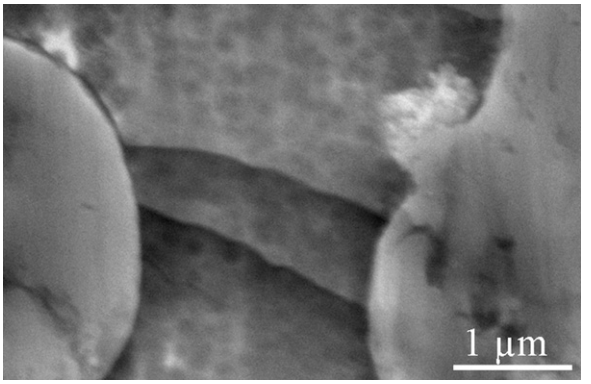

FIG. 6. A scanning electron micrograph, obtained from DH1 that was subjected to cyclic load of $\Delta K \approx 10$ MPa·m$^{0.5}$, showing shear bands confined within two dendrites. Contrast variations are the result of etching.

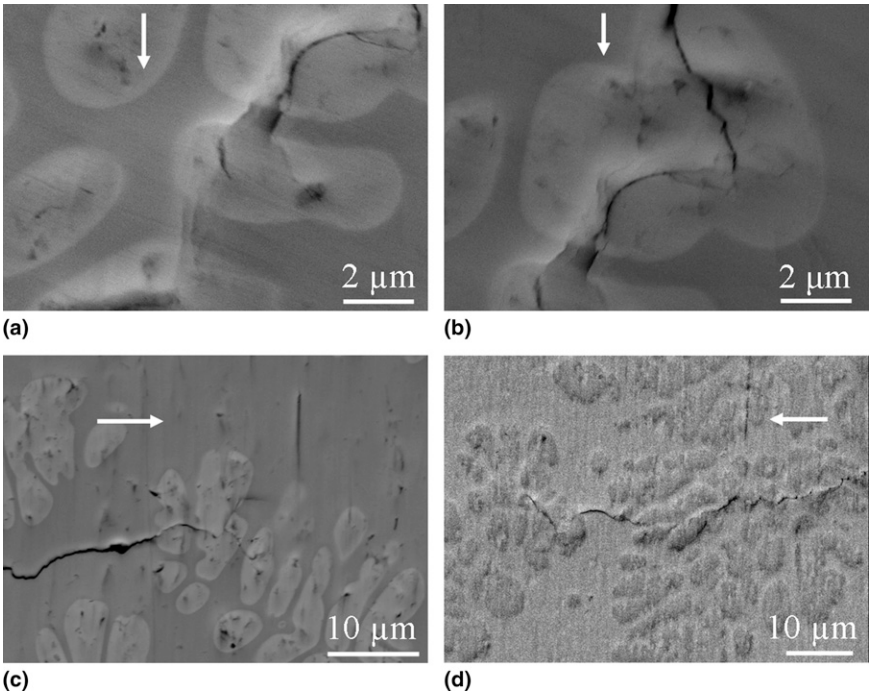

FIG. 7. Scanning electron micrographs, taken in the backscattered mode, obtained near the threshold limit in fatigue-crack propagation in the composites, showing that the crack propagation is effectively hindered by the ductile dendrites through (a, c) crack arrest or (b, d) crack branching. (a, b) are from alloy DH1, (c) is from DH1A, and (d) is from DH1B. Arrow indicates the crack growth direction.

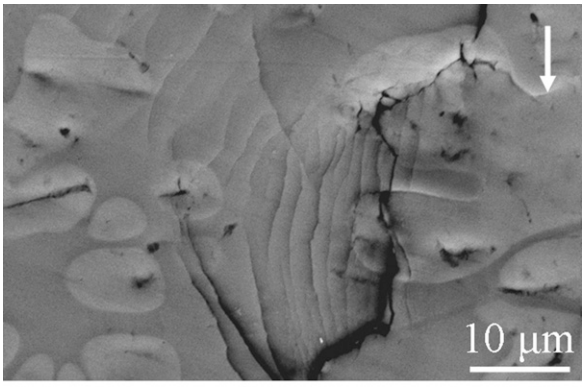

(a)

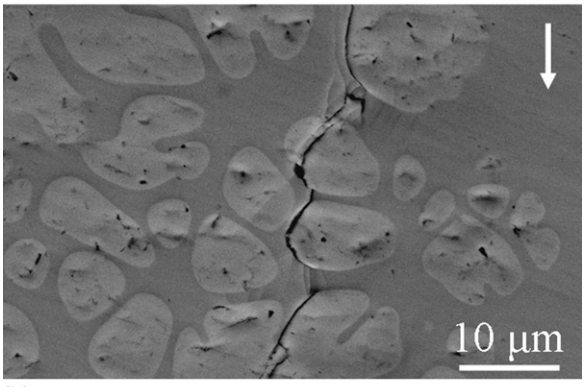

(b)

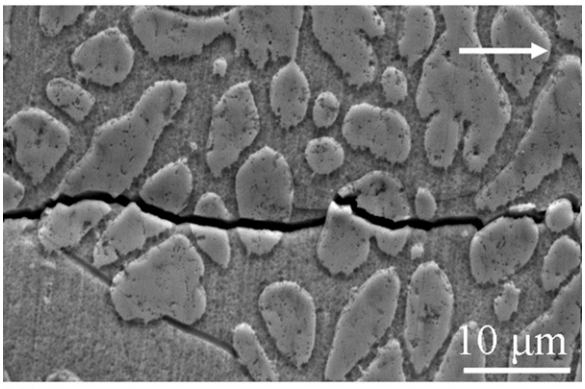

(c)

FIG. 8. Scanning electron micrographs obtained from BMG composite samples that were subjected to fatigue crack growth experiments. The crack growth rate here corresponds to that of the Paris regime with applied $\Delta K \approx 0$ to MPa·m$^{1/2}$. (a) Formation of several shear bands in DH1, parallel to the direction of the crack growth, in the matrix and crack propagation through one of them. (b) A crack meandering around the dendrites by propagating through the matrix/dendrite interface in DH1. (c) Image obtained in the secondary electron image mode on an etched surface of DH1B showing that the fatigue crack passes through the dendrite when the crack makes high incidence angle with interface. Arrows indicate crack growth direction.

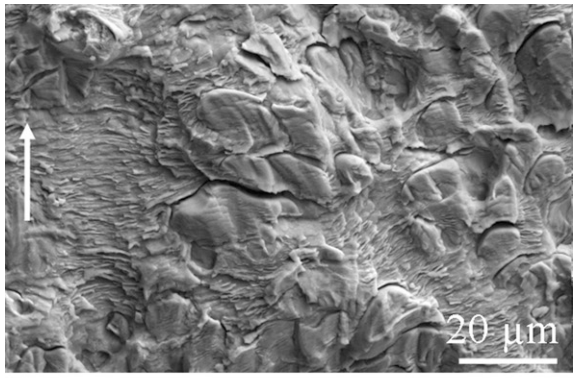

(a)

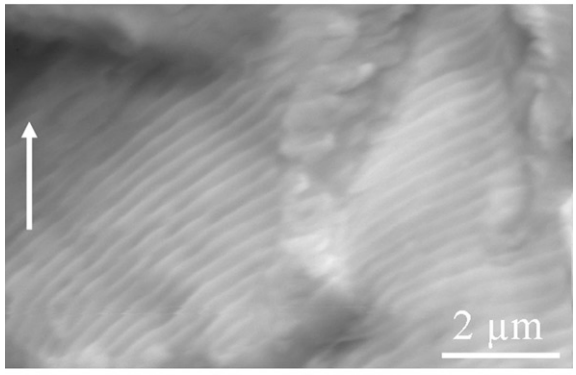

(b)

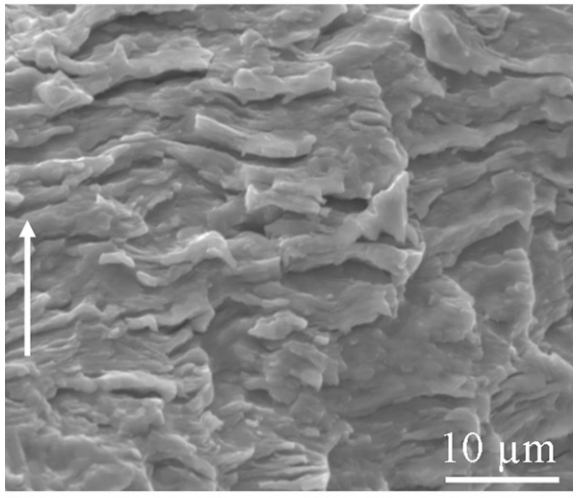

(c)

FIG. 9. Fractographs obtained from the fatigue fractured surfaces of the BMG composites showing (a) low-magnification fracture morphologies of the matrix and the dendrite, and (b, c) fatigue striations in the dendrite and the amorphous matrix, respectively. Note that the striation spacing is much larger in the matrix than in the dendrite, indicating the crack growth rate in the former is much higher. Also note extensive debonding of the dendrites along the matrix/dendrite interface, which could possibly have occurred after the crack has passed through, suggesting tensile residual stresses at the interface.

amorphous matrix [Fig. 9(c)] than in the dendrites. On measuring striations spacing on dendrites at a particular ΔK, it is found that the crack growth rate matches well with striation spacing. For example, the striation spacing in the dendrite when the applied $\Delta K \approx 16$ MPa·m$^{1/2}$ is approximately 0.16 μm, which is equal to the crack growth rate, 1.5×10^{-7} m/cycle in the Zr-based DH1B composite. This result confirms that the fatigue crack growth in the BMG composites is controlled by the

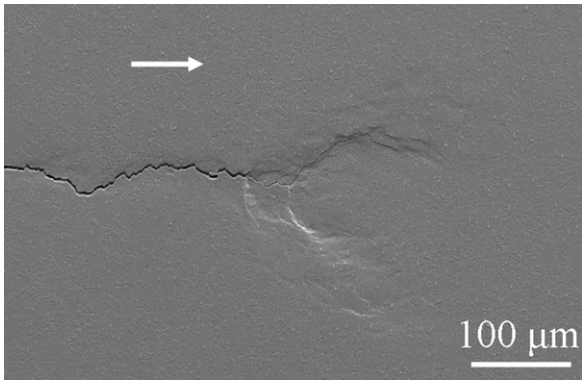

FIG. 10. Typical image showing the development of an extensive plastic zone ahead of the crack tip at high stress intensity factor range. Arrow indicates the crack growth direction.

dendrites, since the crack growth rate is much slower in them than in the amorphous matrix.

At the higher end of the Paris regime, the growing crack develops a large plastic zone as shown in Fig. 10. This is a similar result to what has been shown in quasi-static fracture toughness tested samples[18] and fatigue samples[20] of DH1. Since the specimen size is small, both in terms of thickness as well uncracked ligament length, a plastic hinge develops and the data obtained are no longer valid in the context of fracture mechanics. At that juncture, the fatigue tests were stopped and the samples were broken under quasi-static loads for fractography.

IV. DISCUSSION

The experimental results presented in the preceding section show that the fatigue crack growth resistance of the BMG composites is far superior to that of the monolithic BMG. It is also evident that the dendrites, which are considerably softer than the amorphous matrix, are the cause of the enhanced fatigue crack growth resistance through crack blunting, which arises because of the relatively easy plastic flow and slow crack growth rate in the crystalline dendrites. Despite having different yield strengths, Fig. 5 demonstrates that the change in chemical composition among these composites does not significantly affect ΔK_0 or crack growth rates in the Paris regime. Launey et al.[20] recently reported high fatigue limit compared with the monolithic BMG for a similarly processed composite, DH3, which has 67 vol% of dendrites (as opposed to ~40% in this study). While the fatigue life of monolithic BMGs is primarily decided by the early nucleation of shear bands under cyclic loads and the subsequent propagation of them to form first microcracks and then macrocracks that ultimately lead to catastrophic fracture. The presence of uniformly spaced dendrites in the BMG matrix composites prevents such mechanisms from operating and hence impart a higher ΔK_0, which in turn enables these composites to tolerate even a sizable defect.

Flores et al.[18] reported that ΔK_0 of BMG composites with 25 vol% of second phase is 1.24 MPa·m$^{1/2}$, and yet our measured values are nearly five times that, on similar composites. We think that the marked improvement in ΔK_0 is not caused by the difference in sample dimensions (compact tension versus four-point bending), but rather by the length scale of the microstructure. As noted by Hofmann et al.,[15] toughening and ductility can only be achieved when the length scale of the dendrites matches the length scale at which a shear band transforms into a mixed mode crack. If the dendrite volume fraction is too low or if, more importantly, the size of the dendrites is too small, shear band arrest does not occur. This is most likely the cause of the lower threshold stress intensity of the BMG matrix composite, LM2, tested in Ref. 18, despite having similar microstructure and composition. It appears that the semisolid processing strategy for coarsening the microstructure is far more important for fatigue enhancement than whether the composites are Ti-based or Zr-based.

The Paris exponents of the BMG matrix composites are in the range of 2.6 to 3.7, with the Ti-based alloy DH1A having the smaller value and the Zr-based alloy DH1B having the larger. As mentioned previously, typical Paris exponents for ductile metals lie in the range of 2 to 4. An exponent of 2 can be rationalized using the geometric model that is based on crack-tip blunting and hence cyclic crack tip opening displacement.[17] On the other hand, an exponent of 4 suggests progressive damage accumulation ahead of crack tip through plastic straining. It is interesting to note that the reported values of m for Vitreloy 1 and the BMG matrix composite LM2 are close to 2.[18,25] This suggests that in both these materials crack growth is controlled by that of the matrix. In contrast, the m values of the composites tested in this work are much higher (closer to 4 in the case of DH1B) suggesting that these are controlled by progressive damage accumulation.

V. SUMMARY AND CONCLUSIONS

An experimental investigation into the mechanical properties of three engineered BMG matrix composites, which have similar ductile dendrite volume fraction but with varying chemical composition, was conducted. Results show that these composites have considerably higher threshold for fatigue crack growth initiation than monolithic BMGs and other previously reported BMG matrix composites. This was achieved by carefully designing the microstructure length scale of secondary ductile phase, such as dendrite arm spacing and interdendrite length, to constrain the shear bands and arrest propagating

cracks. The Paris exponent, m, in the crack growth regime is in a similar range to ductile crystalline materials. Fatigue striations in the dendrite and glass matrix exemplify that the primary crack growth mechanism is blunting and resharpening of the crack tip. The effect of changing the composition of the composites from Zr-based to Ti-based appears to have little effect on the fatigue characteristics. Although both the Ti-based and Zr-based BMG matrix composites have been shown to have >10% tensile ductility, they have much different fracture toughness values. Zr-based composites with ~60% glass phase (DH1) have been shown[15] to have $K_{Ic} \approx 100$ MPa·m$^{1/2}$ while Ti-based BMG composites with ~60% glass phase (DV1) have been shown[22] to have $K_{Ic} \approx 50$ MPa·m$^{1/2}$. It seems that the lower density of the Ti-based alloys has a penalty with toughness. However, this work demonstrates that there is little penalty in the fatigue crack growth by moving to a lower density Ti-based composite over a Zr-based one. The scale of the microstructure of the two phases is the critical component.

REFERENCES

1. C.A. Schuh, T.C. Hufnagel, and U. Ramamurty: Mechanical behavior of amorphous alloys. *Acta Mater.* **55,** 4067 (2007).
2. C.J. Gilbert, V. Schroeder, and R.O. Ritchie: Mechanisms for fracture and fatigue-crack propagation in a bulk metallic glass. *Metall. Mater. Trans. A* **30,** 1739 (1999).
3. R. Raghavan, R. Ayer, H.W. Jin, C.N. Marzinsky, and U. Ramamurty: Effect of shot peening on the fatigue life of a Zr-based bulk metallic glass. *Scr. Mater.* **59,** 167 (2008).
4. R. Bhowmick, R. Raghavan, K. Chattopadhyay, and U. Ramamurty: Plastic flow softening in a bulk metallic glass. *Acta Mater.* **54,** 4221 (2006).
5. B.G. Yoo, K.W. Park, J.C. Lee, U. Ramamurty, and J. Jang: Role of free volume in strain softening of as-cast and annealed bulk metallic glass. *J. Mater. Res.* **24,** 1405 (2009).
6. N. Nagendra, U. Ramamurty, T.T. Goh, and Y. Li: Effect of crystallinity on the impact toughness of a La-based bulk metallic glass. *Acta Mater.* **48,** 2603 (2000).
7. J. Basu, N. Nagendra, Y. Li, and U. Ramamurty: Microstructure and mechanical properties of partially-crystallized La-based bulk metallic glass. *Philos. Mag.* **83,** 1747 (2003).
8. R. Raghavan, P. Murali, and U. Ramamurty: On the factors influencing the ductile to brittle transition in a bulk metallic glass. *Acta Mater.* **57,** 3332 (2009).
9. R. Raghavan, V.V. Shastry, A. Kumar, T. Jayakumar, and U. Ramamurty: Toughness of as cast and partially recrystallized Zr-based bulk metallic glass. *Intermetallics* **17,** 835 (2009).
10. T. Liu, P. Shen, F. Qiu, Z. Yin, Q. Lin, Q. Jiang, and T. Zhang: Synthesis and mechanical properties of TiC-reinforced Cu-based bulk metallic glass composites. *Scr. Mater.* **60,** 84 (2009).
11. C.C. Hays, C.P. Kim, and W.L. Johnson: Microstructure controlled shear band pattern formation and enhanced plasticity of bulk metallic glasses containing in situ formed ductile phase dendrite dispersions. *Phys. Rev. Lett.* **84,** 2901 (2000).
12. F. Szuecs, C.P. Kim, and W.L. Johnson: Mechanical properties of $Zr_{56.2}Ti_{13.8}Nb_{5.0}Cu_{6.9}Ni_{5.6}Be_{12.5}$ ductile phase reinforced bulk metallic glass composite. *Acta Mater.* **49,** 1507 (2001).
13. Z. Bian, H. Kato, C. Qin, W. Zhang, and A. Inoue: Cu–Hf–Ti–Ag–Ta bulk metallic glass composites and their properties. *Acta Mater.* **53,** 2037 (2005).
14. C.L. Qin, W. Zhang, K. Asami, H. Kimura, X.M. Wang, and A. Inoue: A novel Cu-based BMG composite with high corrosion resistance and excellent mechanical properties. *Acta Mater.* **54,** 3713 (2006).
15. D.C. Hofmann, J.Y. Suh, A. Wiest, G. Duan, M.L. Lind, M.D. Demetriou, and W.L. Johnson: Designing metallic glass matrix composites with high toughness and tensile ductility. *Nature* **451,** 1086 (2008).
16. M.E. Launey, D.C. Hofmann, J.Y. Suh, H. Kozachkov, W.L. Johnson, and R.O. Ritchie: Fracture toughness and crack-resistance curve behavior in metallic glass-matrix composites. *Appl. Phys. Lett.* **94,** 241910 (2009).
17. S. Suresh: *Fatigue of Materials*, 2nd ed. (Cambridge University Press, Cambridge, 1998).
18. M. Flores, W.L. Johnson, and R.H. Dauskardt: Fracture and fatigue behavior of a Zr–Ti–Nb ductile phase reinforced bulk metallic glass matrix composite. *Scr. Mater.* **49,** 1181 (2003).
19. G.Y. Wang, P.K. Liaw, A. Peker, M. Freels, W.H. Peter, R.A. Buchanan, and C.R. Brooks: Comparison of fatigue behavior of a bulk metallic glass and its composite. *Intermetallics* **14,** 1091 (2006).
20. M.E. Launey, D.C. Hofmann, W.L. Johnson, and R.O. Ritchie: Solution to the problem of the poor cyclic fatigue resistance of bulk metallic glasses. *Proc. Nat. Acad. Sci. U.S.A.* **106,** 4986 (2009).
21. G. Subhash, R.J. Dowding, and L.J. Kecskes: Characterization of uniaxial compressive response of a bulk amorphous Zr–Ti–Cu–Ni–Be alloy. *Mater. Sci. Eng., A* **234,** 33 (2002).
22. D.C. Hofmann, J.Y. Suh, A. Wiest, M.L. Lind, M.D. Demetriou, and W.L. Johnson: Development of tough, low-density titanium-based bulk metallic glass matrix composites with tensile ductility. *Proc. Nat. Acad. Sci. U.S.A.* **105,** 20136 (2008).
23. Standard test method for measurement of fatigue crack-growth rates. E 647-05. (ASTM International, W. Conshohocken, PA, 2005), p. 1–45.
24. A. Leonhard, L.Q. Xing, M. Heilmaier, A. Gebert, J. Eckert, and L. Schultz: Effect of crystalline precipitations on the mechanical behavior of bulk glass forming Zr-based alloys. *Nanostruct. Mater.* **10,** 805 (1998).
25. H. Zhang, Z.G. Wang, K.Q. Qiu, Q.S. Zang, and H.F. Zhang: Cyclic deformation and fatigue crack propagation of a Zr-based bulk amorphous metal. *Mater. Sci. Eng., A* **356,** 173 (2003).